Electronic Supplementary Material (ESI) for Materials Horizons.

Supporting Information

Growth of a dense Gadolinium metal-organic framework on oxide-free Silicon for cryogenic local refrigeration

*Giulia Lorusso, Eva Natividad, Marco Evangelisti and Olivier Roubeau**

TABLE OF CONTENTS

A) Powder X-ray diffraction

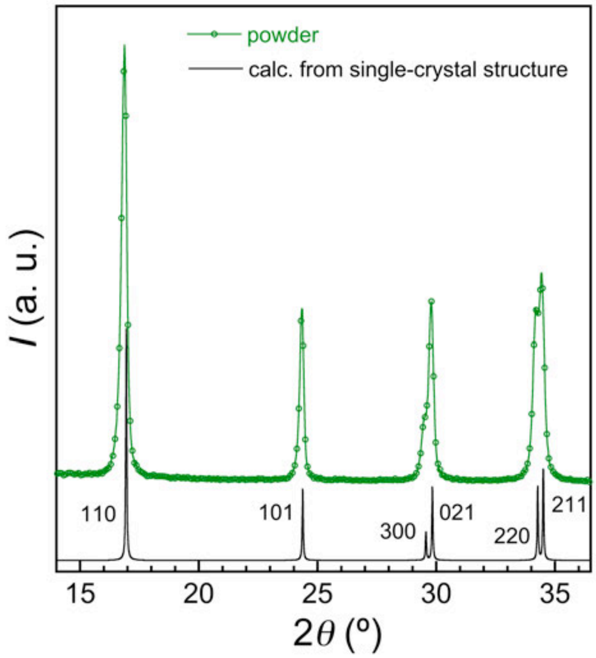

Figure S1. Powder X-ray diffraction patterns of the polycrystalline powder of Gd(HCOO)$_3$ used in this work, compared with the patterns calculated from the reported single-crystal structure.

B) Contact angle measurements

Static water contact angles were determined using a home-made set-up with an estimated accuracy of ±3° (Milli-Q water, 3 droplets per substrate). The set-up is simply built on an OLYMPUS SZ-11 optical microscope equipped with a digital camera (OLYMPUS 500UZ + adapter U-PMTVC), and held by an adaptable arm (OLYMPUS SZ-PT, SZ-STB1, SZ-STU1) allowing to rotate it so that droplets of water on the different surfaces are observed horizontally from the side. Measurements were repeated for some of the substrates using an Attension Theta Lite contact angle meter, with an estimated accuracy of 1°, giving similar values.

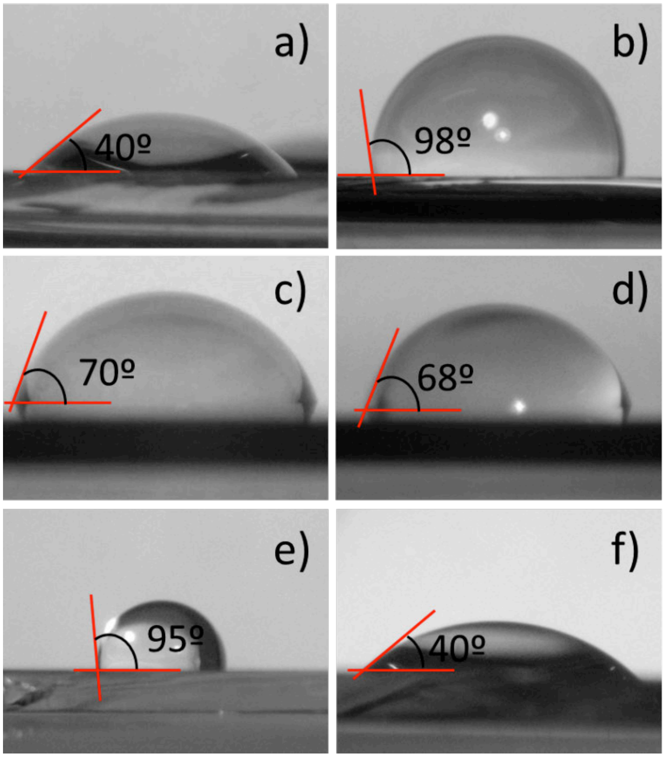

Figure S2. Characteristic static contact angles of MilliQ water droplets on: Si(100) substrate before (a) and after (b) etching of the native oxide layer by dip in HF; (c) etched Si(100) wafer after 24h in MUDA, **1(C_{11})**; (d) etched Si(100) wafer after 24h in MHDA, **1(C_{16})**; (e) Si(100)/Cr/Au substrate and (f) Si(100)/Cr/Au after 24h in MUDA, **1**^{Au}**(C_{11})**.

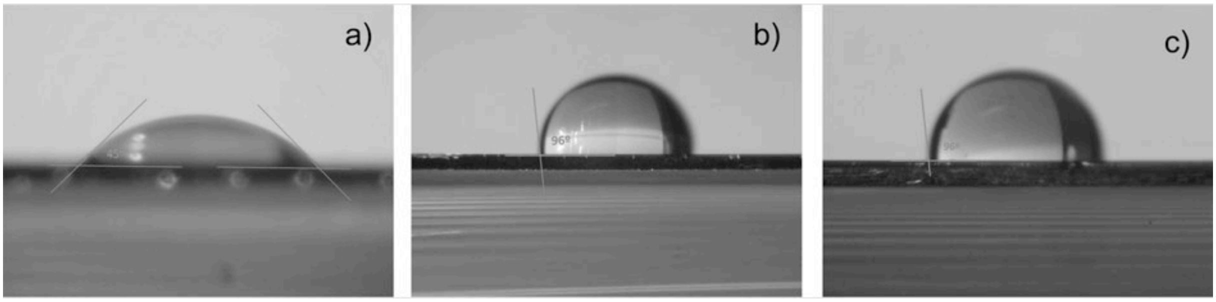

Figure S3. Characteristic static contact angles of MilliQ water droplets on: Si(111) substrate after hydrosilylation with a) undecenoic acid, **2**; b) undecene, **2**^{ref}; c) dodecyne, **3**^{ref}.

C) X-ray Photo-electron Spectroscopy

X-ray Photoelectron Spectroscopy measurements were performed in a Kratos AXIS SUPRA spectrometer, using a monochromatized Al Ka source (1486.6 eV) at the Laboratorio de Microscopías Avanzadas (LMA). Wide scans were acquired at analyzer pass energy of 160 eV, whereas high-resolution narrow scans were performed at constant pass energy of 20 eV. The spectra were obtained at room temperature. The binding energy (BE) scale was internally referenced to the C 1s peak (BE for CC = 284.9 eV). All processing and fitting was done with CasaXPS software.

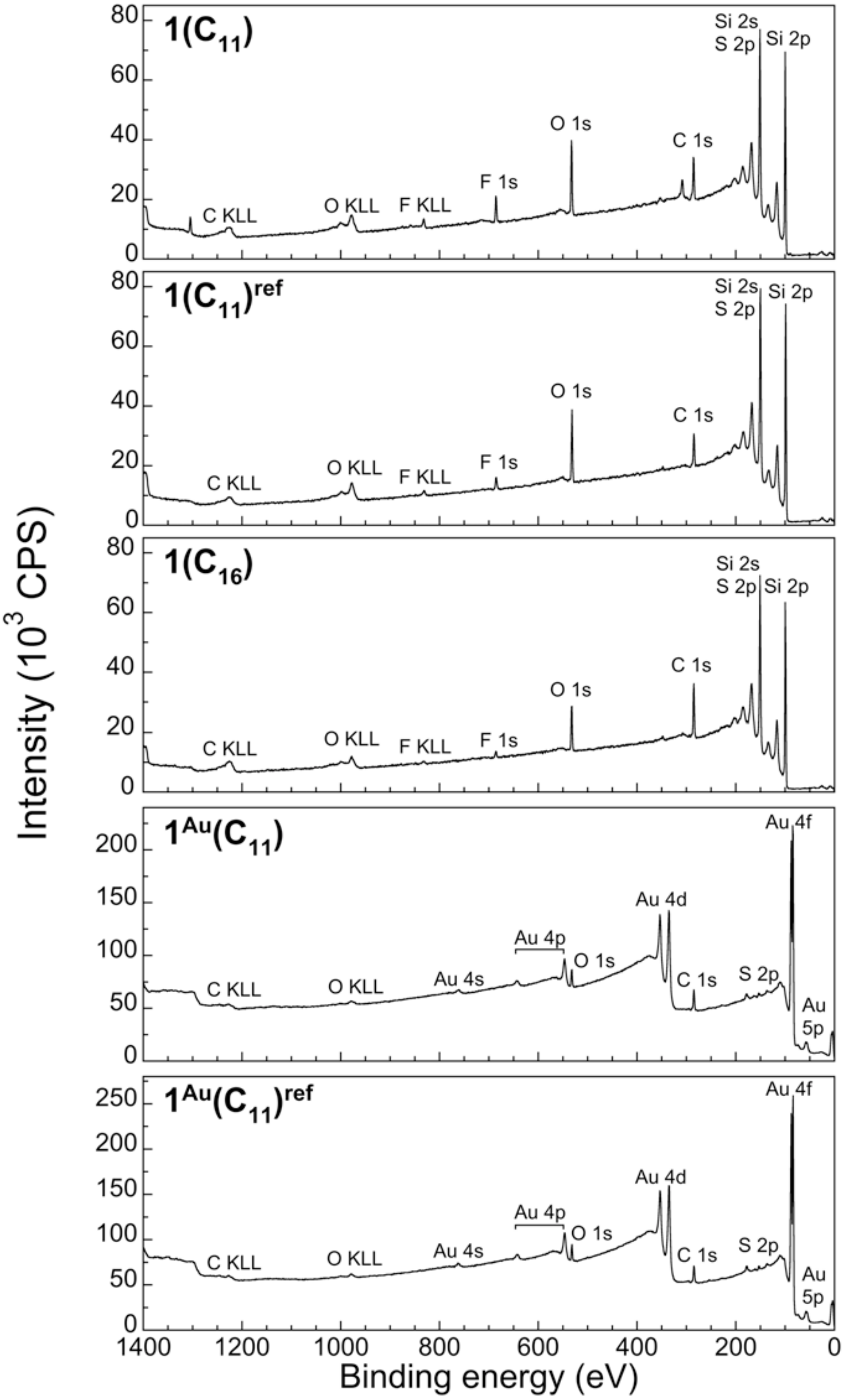

Figure S4. XPS survey spectra for the used thiol-based SAMs on oxide-free Si, as indicated.

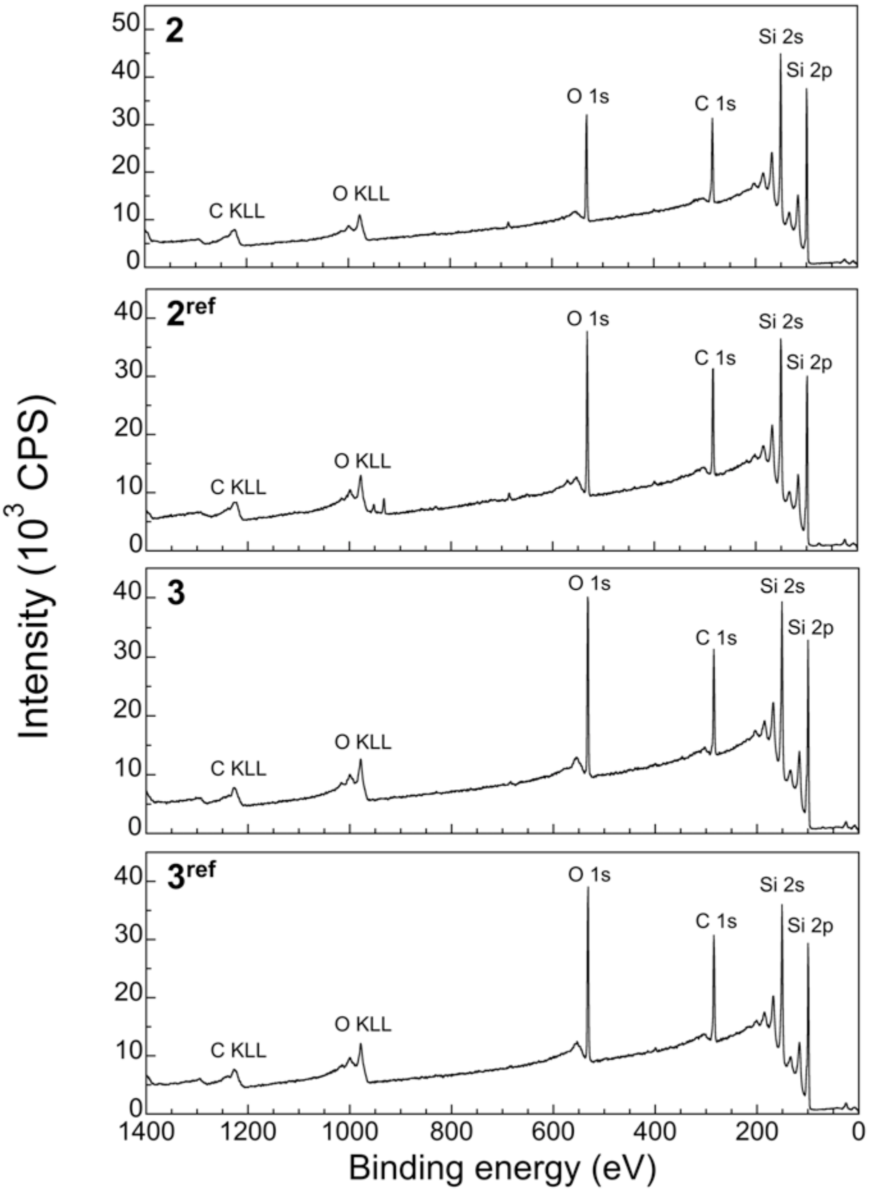

Figure S5. XPS survey spectra for the used hydrosilylated covalent SAMs on oxide-free Si(111), as indicated.

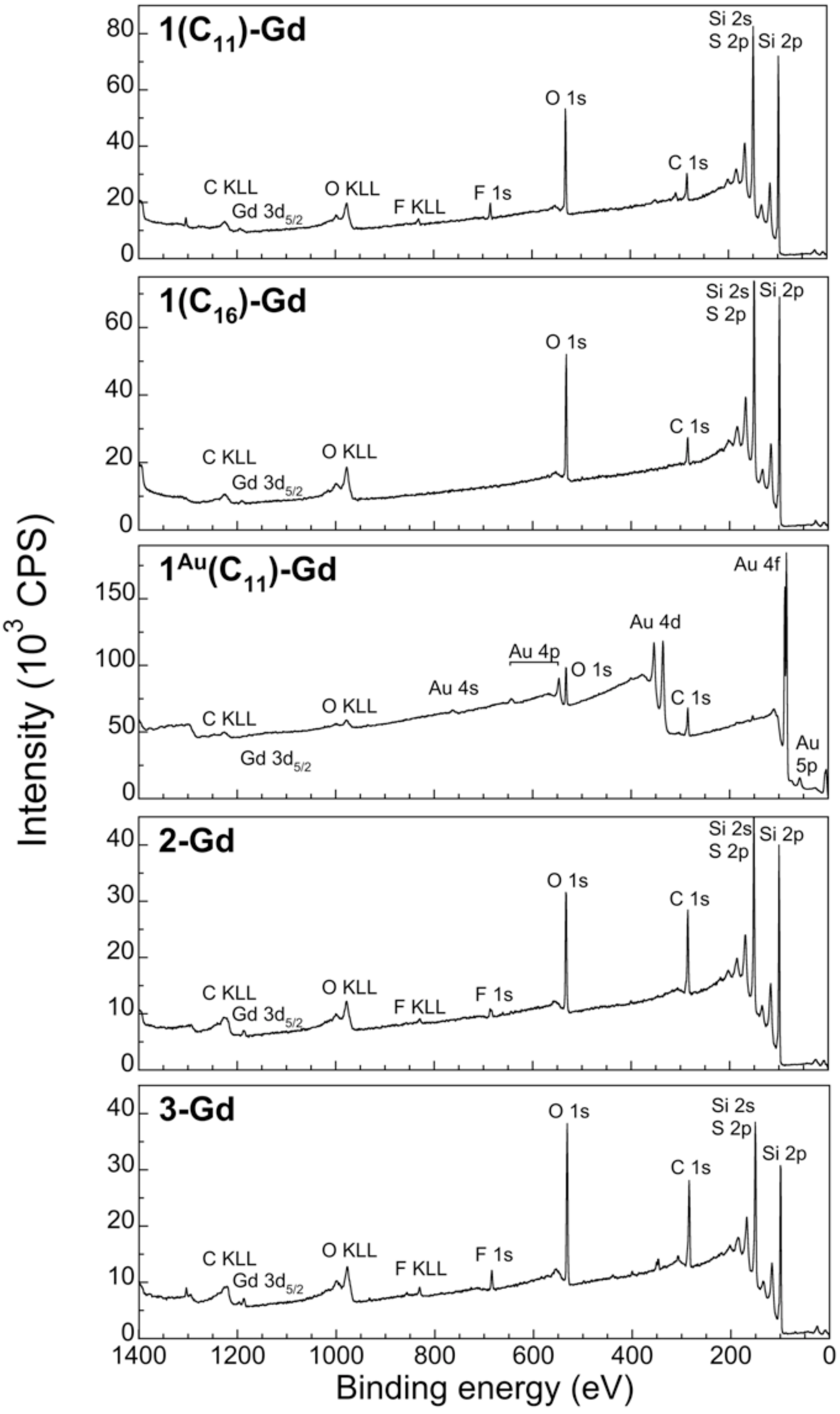

Figure S6. XPS survey spectra for the grown Gd(formate)$_3$ material on various carboxylate-terminated SAMs, as indicated.

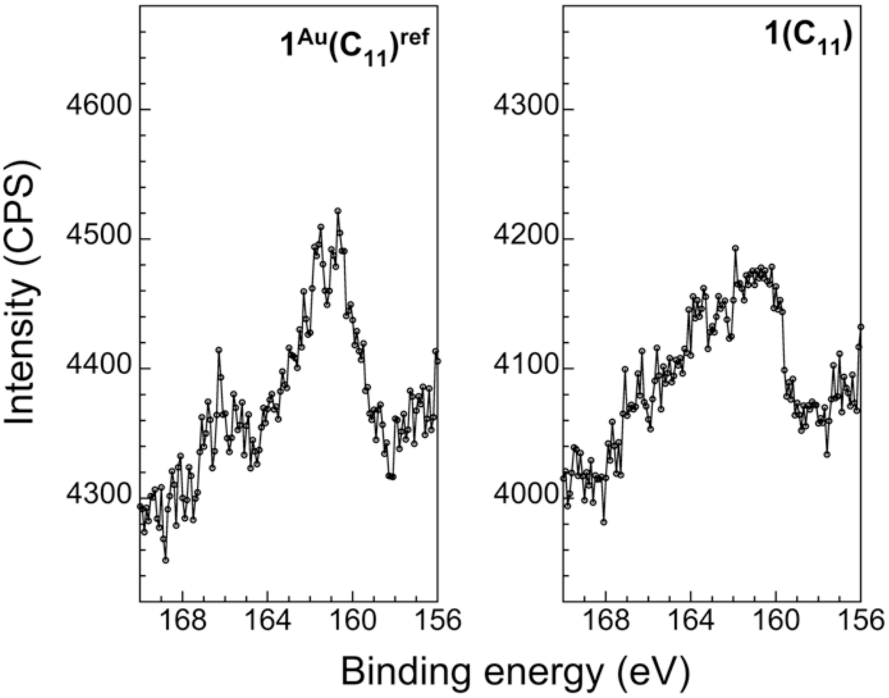

Figure S7. High resolution XPS spectra of the S 2p region for the thiol-based SAMs $\mathbf{1^{Au}(C_{11})^{ref}}$ and $\mathbf{1(C_{11})}$.

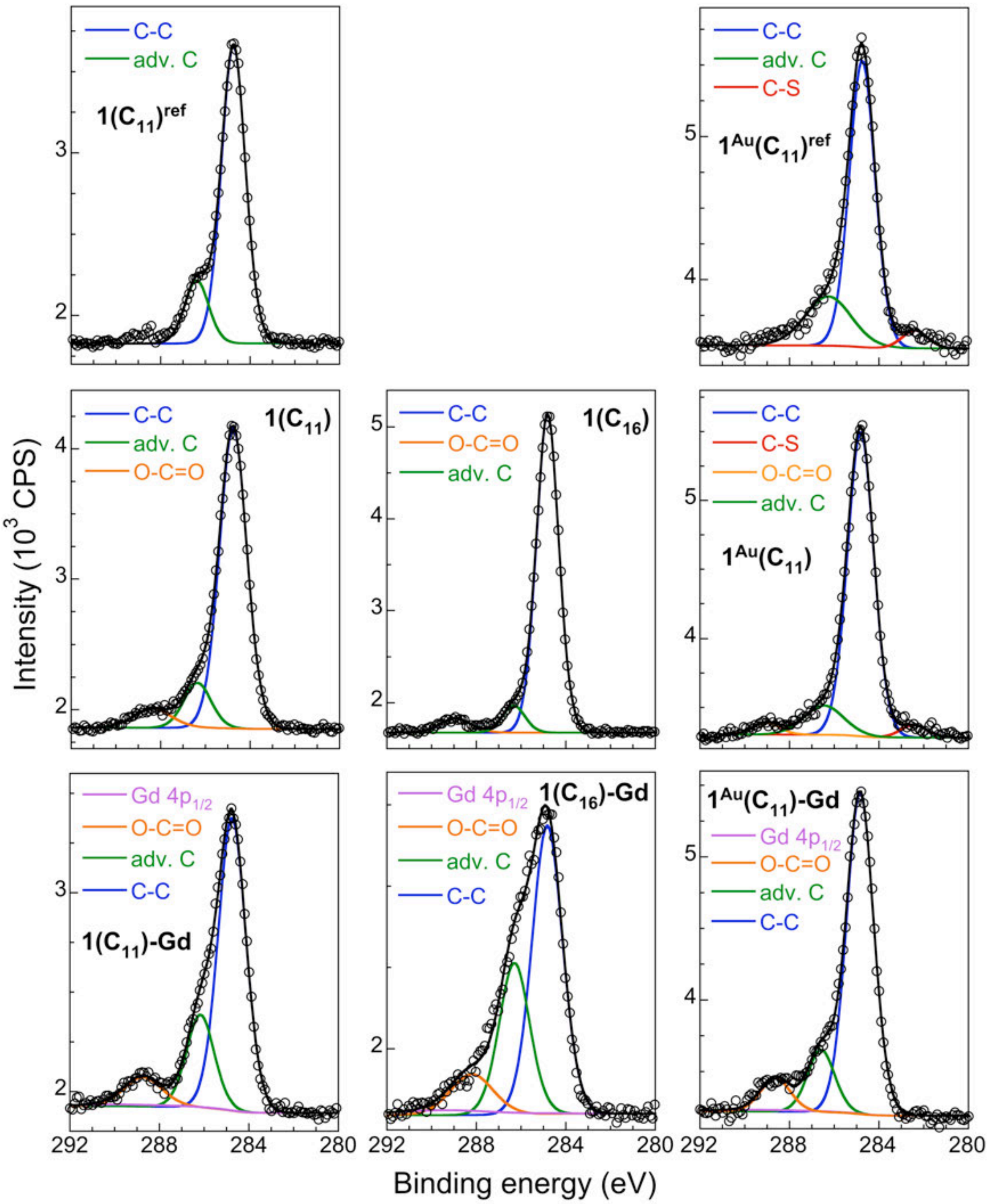

Figure S8. High resolution C 1s XPS spectra for the thiol-based SAMs on oxide-free Si(100) and for the grown Gd(formate)$_3$ material on various carboxylate-terminated SAMs, as indicated.

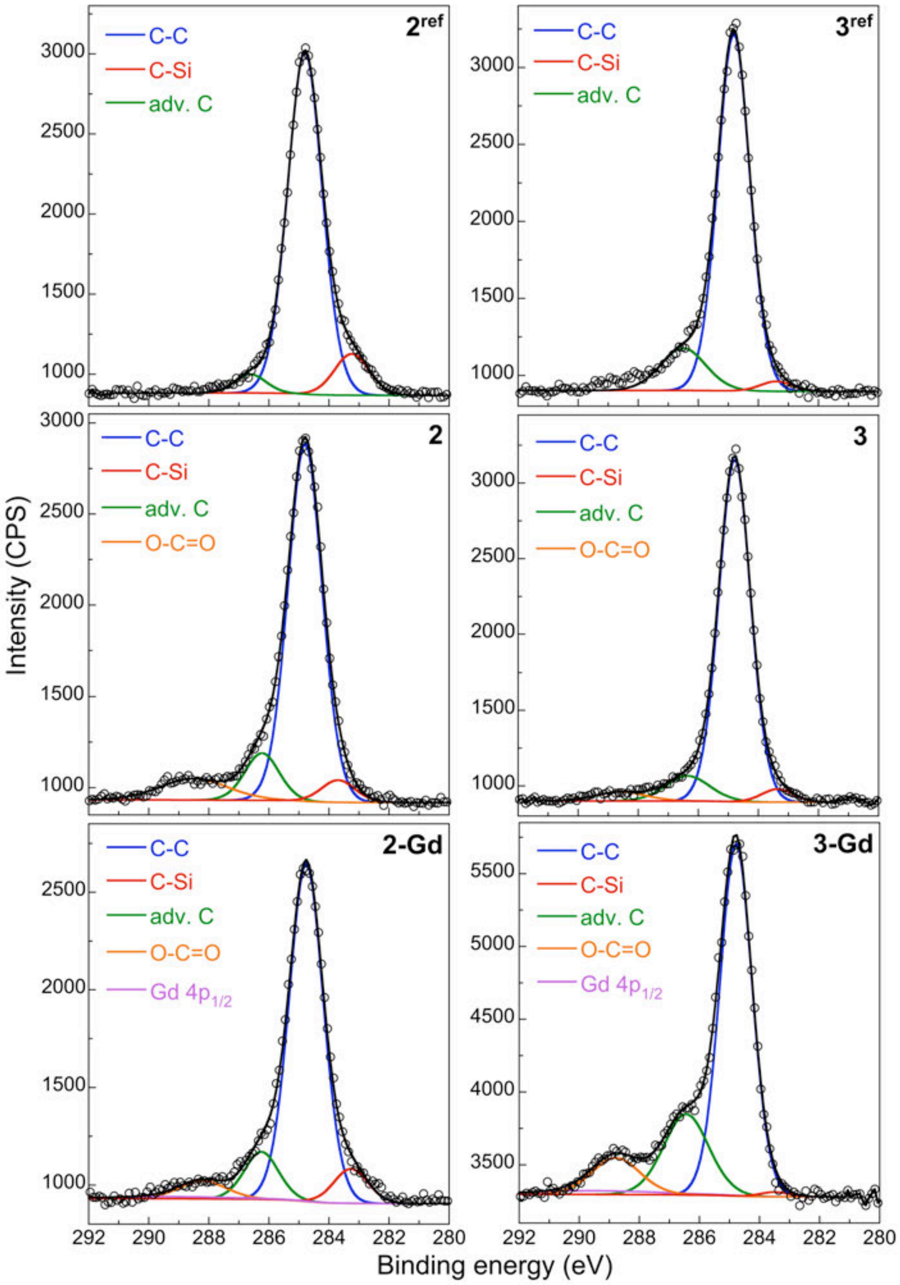

Figure S9. High resolution C 1s XPS spectra for the covalent hydrosilylated SAMs on oxide-free Si(111) and for the grown Gd(formate)$_3$ material on the carboxylate-terminated ones, as indicated.

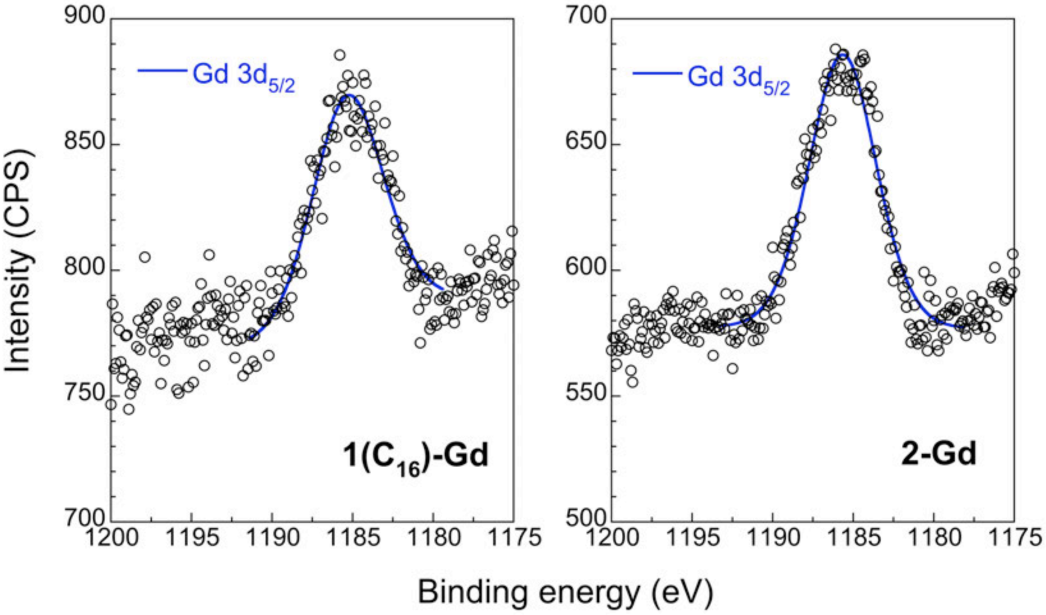

Figure S10. High resolution XPS spectra of the Gd 3d region for **1(C_{16})-Gd** and **2-Gd**.

D) Field-Emission Scanning Electron Microscopy of grown Gd(formate)$_3$ MOF

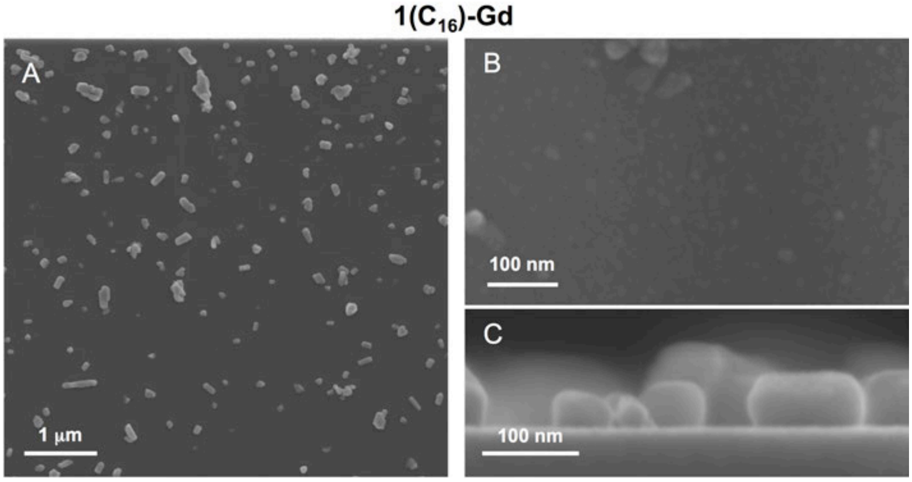

Figure S11. Characteristic FESEM images of the Gd(formate)$_3$ MOF grown on thiol-based SAM on oxide-free Si(100) (**1(C$_{16}$)-Gd**).

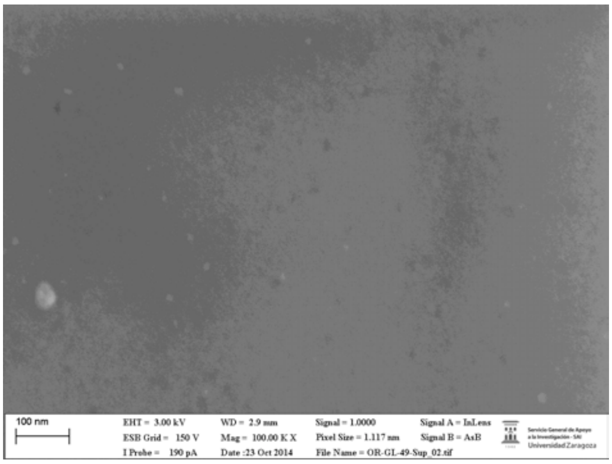

Figure S12. Characteristic FESEM image of an undecanethiol SAM on oxide-free Si(100) after 24h immersion in an ethanol solution of Gd(formate)$_3$ (**1(C$_{11}$)^{ref}-Gd**), showing the absence of the thin layer of rounded objects observed in the case of carboxylic acid SAMs in **1(C$_{11}$)-Gd**, **1(C$_{16}$)-Gd** and **1^{Au}(C$_{11}$)-Gd**. Note however that a few isolated large nanocrystals are also observed.

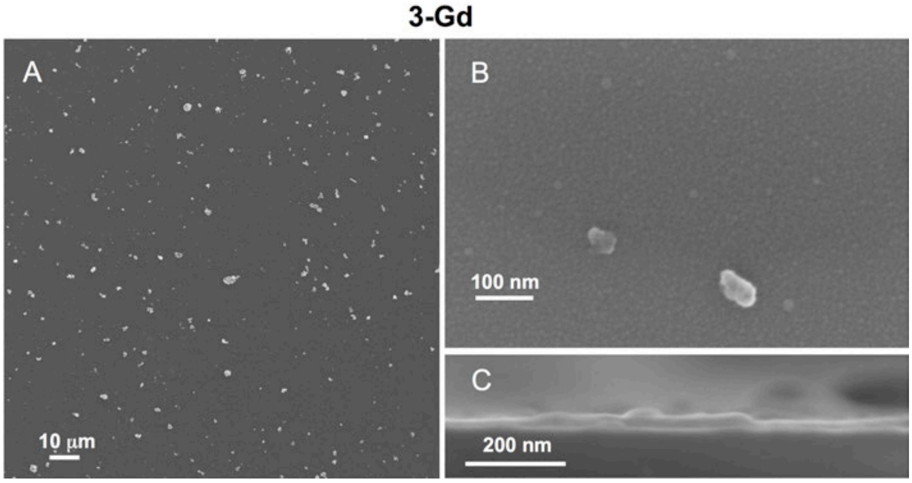

Figure S13. Characteristic FESEM images of the Gd(formate)$_3$ MOF grown on covalent monolayer obtained by hydrosilylation of Si(111) with an alkyne (**3-Gd**).

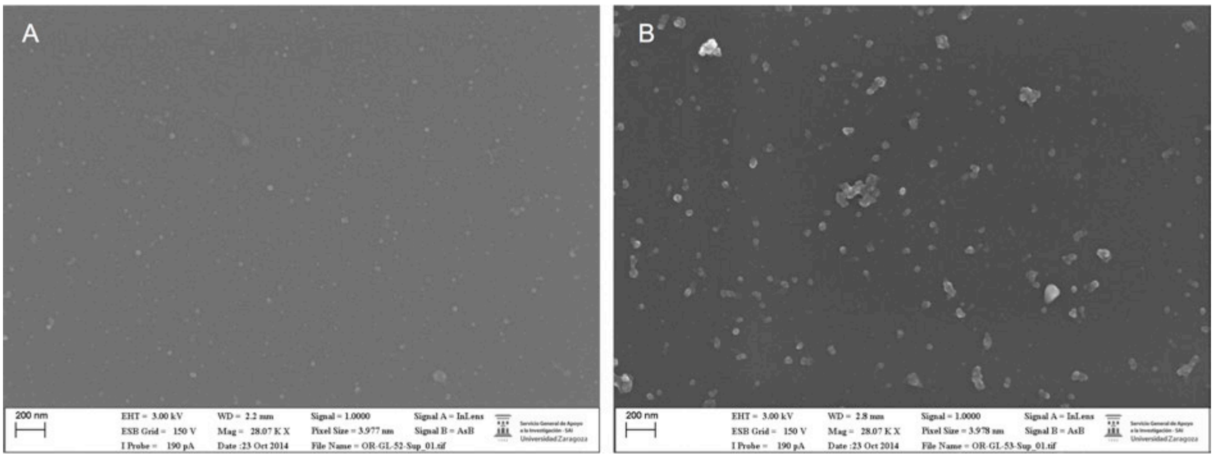

Figure S14. Characteristic FESEM images of the Gd(formate)$_3$ MOF grown on thiol-based SAM on oxide-free Si(100) using a 10-fold diluted solution: A) on **1(C_{11})** and B) on **1(C_{16})**

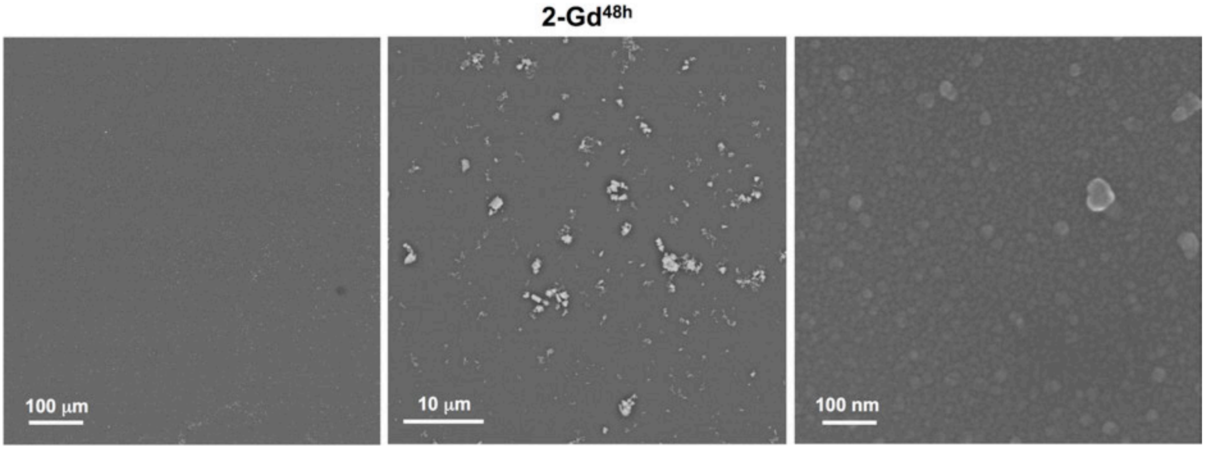

Figure S15. Characteristic FESEM images of the Gd(formate)$_3$ MOF grown with a longer 48h immersion on covalent monolayer obtained by hydrosilylation of Si(111) (**2-Gd^{48h}**).

E) Atomic Force Microscopy of monolayers

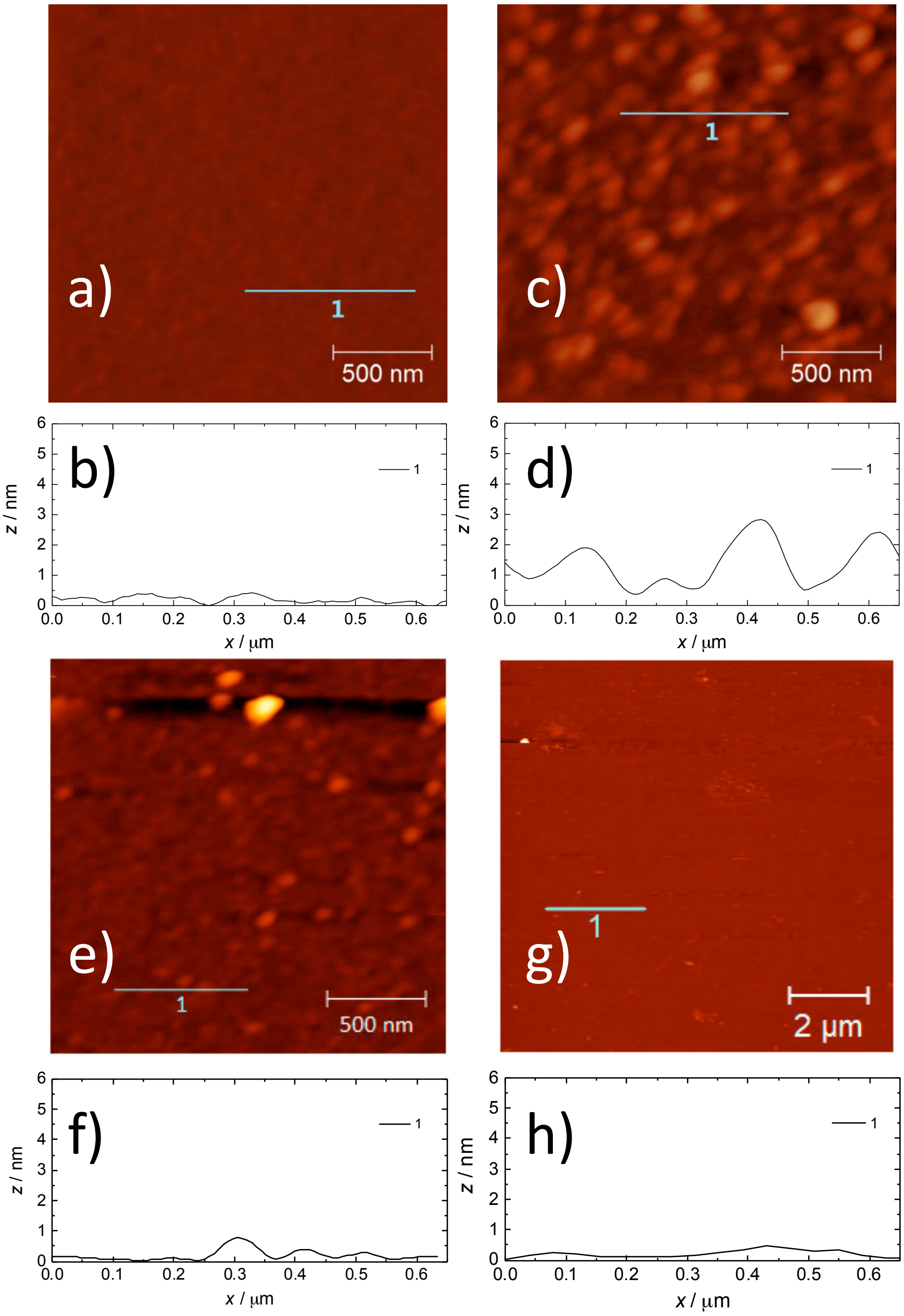

Figure S16. Characteristic AFM topography images and relative surface profiles for the bare oxide-free Si(100) surface (a,b), **1(C$_{11}$)** (c,d), **1(C$_{16}$)** (e, f) and **1(C$_{11}$)^{ref}** (g, h) SAMs.

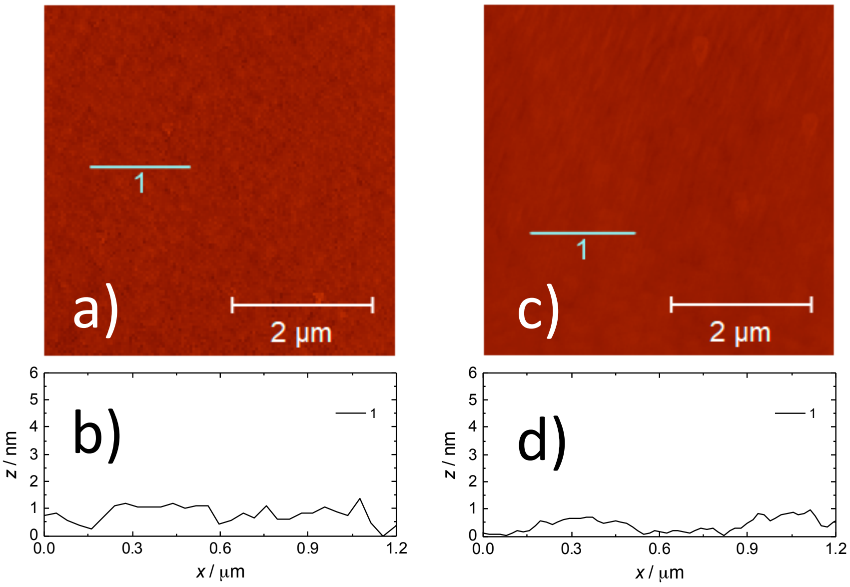

Figure S17. Characteristic AFM topography images and relative surface profiles for the bare Au-coated Si(100) substrate (a, b) and $\mathbf{1^{Au}(C_{11})}$ (c, d) SAM.

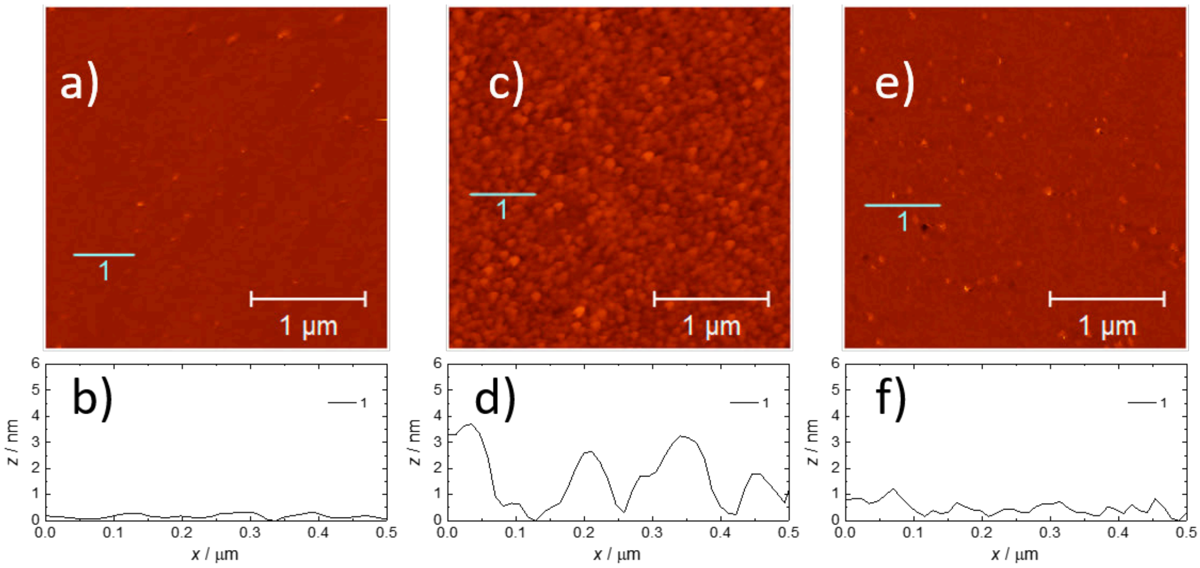

Figure S18. Characteristic AFM topography images and relative surface profiles for the bare oxide-free Si(111) surface (a, b), **2** (c, d) and **3** (e, f) monolayers.

F) Magnetic properties

The following describes the method used to determine the magnetic properties of the Gd(formate)$_3$ films grown on the different Si substrates expressed in molar or mass units per surface area. This is illustrated with the sample with the lowest signal, **1(C$_{11}$)-Gd**.

First the raw *M vs. H* data obtained for the piece of Si wafer covered with the grown film (here **1(C$_{11}$)-Gd**) is corrected of the signal corresponding to the Si wafer. For this the *M vs. H* data obtained for the untreated Si wafer (**1(C$_{11}$)**) is normalized to the actual area of the sample (here 0.25 cm^2) and subtracted to the raw data. This provides with the raw magnetization of the grown film in **1(C$_{11}$)-Gd**.

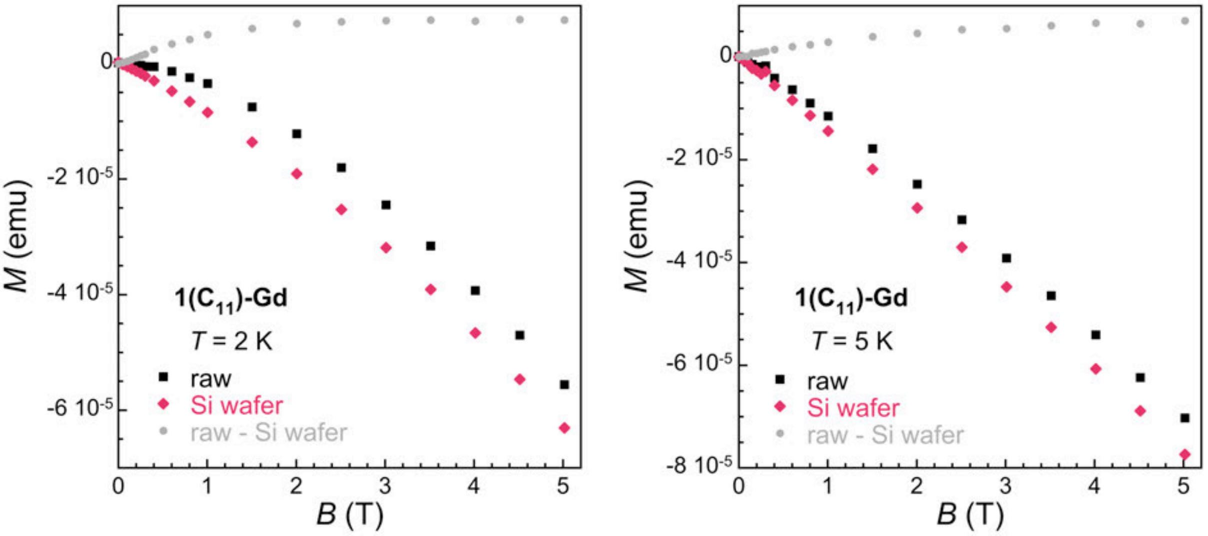

Figure S19. Raw magnetization *vs*. field data at 2 (left) and 5 K (right) for **1(C$_{11}$)-Gd** (black squares) and the untreated Si wafer (red rhombs), normalized to the area of the **1(C$_{11}$)-Gd** sample. The difference gives the raw magnetization of the grown film of Gd(formate)$_3$ in the measured **1(C$_{11}$)-Gd** sample (grey circles).

Then, the raw magnetization data of the grown film at both 2 and 5 K are multiplied by the same factor so as to agree as much as possible with the corresponding molar *M vs. H* data of the bulk Gd(formate)$_3$, expressed in $N_A\mu_B$ units. In the case of **1(C$_{11}$)-Gd**, this factor amounts to 9.0x10^5 and the agreement is quite good (Figure S19 right).

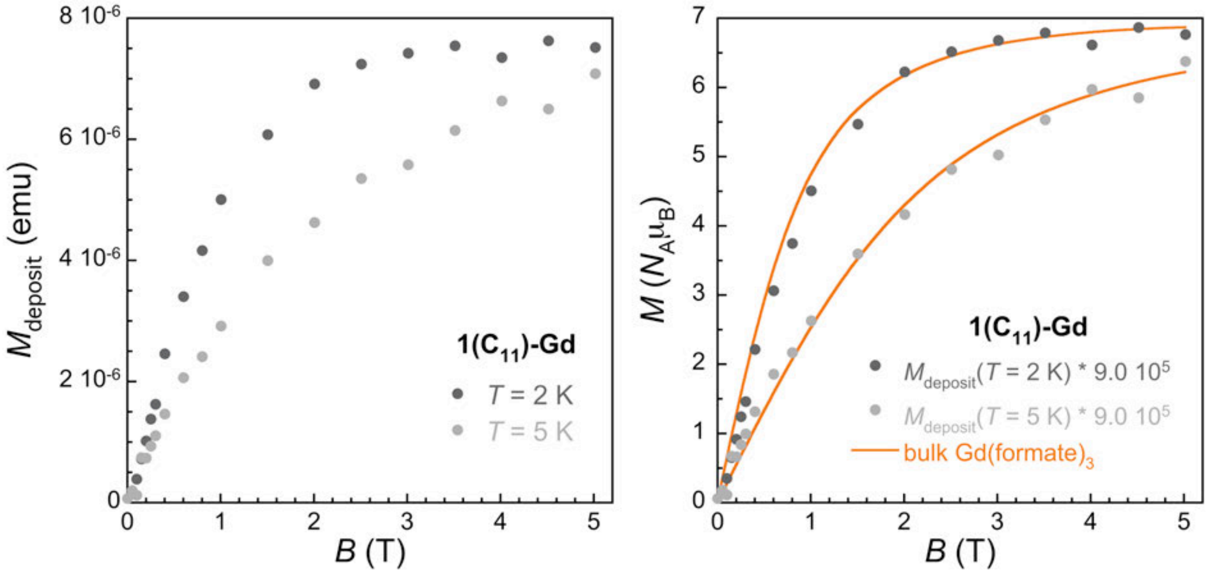

Figure S20. Left: raw magnetization of the grown film of Gd(formate)$_3$ in the measured **1(C$_{11}$)-Gd** sample at 2 and 5 K, as determined in Figure S18. Right: The same magnetization *vs.* field data scaled by the same indicated factor to agree with the molar magnetization *vs.* field data of bulk Gd(HCOO)$_3$ (orange full lines).

This gives an estimation of the amount of Gd(formate)$_3$ of the grown film since the scale factor to go from emu to $N_A m_B$ units is simply the product of $N_A\mu_B$ in cgs units (5585 ergG^{-1}mol^{-1}) by the number of mole of Gd(formate)$_3$. Considering the molar weight of Gd(formate)$_3$ of 292.3 g/mol, this gives in the case of **1(C$_{11}$)-Gd**:

m = 292.3/(9x105*5585) = 0.58x10^{-7} g, rounded to 0.6x10^{-7} g in Table 2.

Eventually, the magnetization and mass of the grown films are reported respectively in Figures 5, S20 and S21 and Table 2 in molar magnetization or mass units per surface area ($N_A\mu_B$ cm^{-2} or g cm^{-2}) using the latter estimation and the area of the measured piece of Si wafer (0.25 cm^2).

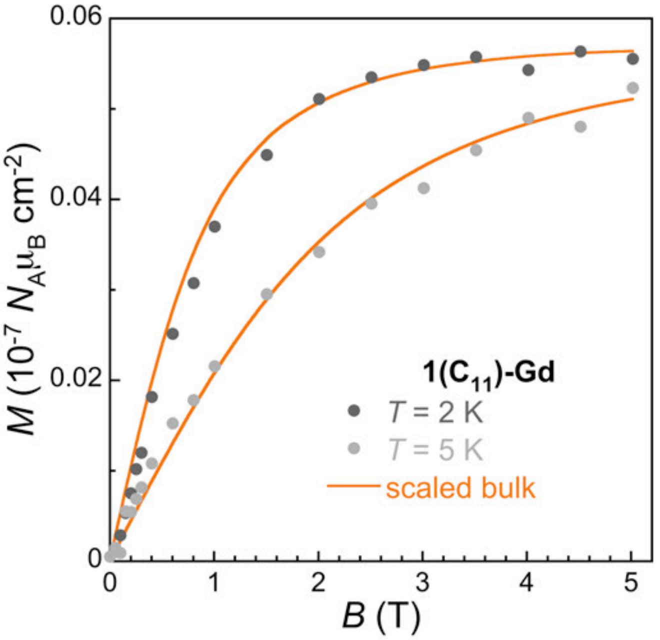

Figure S21. Field dependence of the magnetization per surface area at 2 and 5 K for the grown film of Gd(formate)$_3$ in **1(C$_{11}$)-Gd**. The bulk material data is again shown as orange lines, after scaling by the appropriate factor (*i.e.* the determined number of mole of Gd(formate)$_3$ divided by the area of the sample).

The same procedure was used for variable temperature data using the same scale factor as determined with the magnetization *vs*. field data.

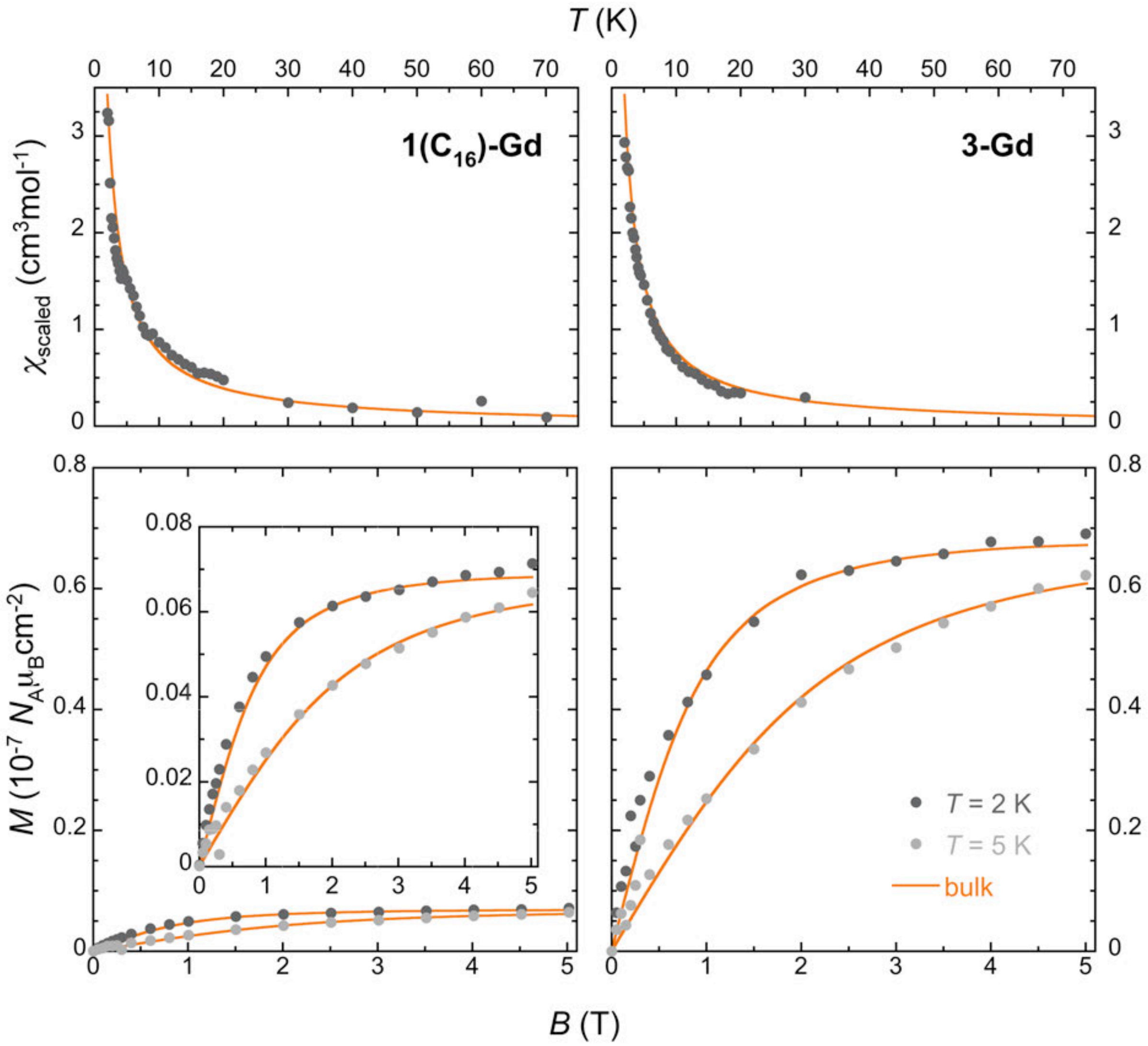

Figure S22. Magnetic properties of the $Gd(HCOO)_3$ thin films grown on oxide-free silicon with different subjacent carboxylic monolayers as indicated. Top: temperature dependence of the molar magnetic susceptibility obtained by scaling to the bulk material data shown as orange lines. Bottom: isothermal field dependence of the magnetization per surface area at 2 and 5 K. In this case, the data is shown without scaling and using the same range to evidence the significant differences arising from the subjacent carboxylate monolayers and growth time. The scaled bulk material data is again shown as orange lines. For **1(C$_{16}$)-Gd**, the data is also shown with a more adequate range as inset.